# Relaxation, Equilibrium Oligomerization, and Molecular Symmetry of the VASP (336−380) EVH2 Tetramer†

Jürgen Zimmermann,*,‡ Dirk Labudde,‡ Thomas Jarchau,§ Ulrich Walter,§ Hartmut Oschkinat,‡ and Linda J. Ball*,‡

*Forschungsinstitut für Molekulare Pharmakologie, Robert-Rössle-Strasse 10, 13125 Berlin, Germany, and Institut für Klinische Biochemie und Pathobiochemie, Universität Würzburg, Versbacher Strasse 5, 97078 Würzburg, Germany*

*Received May 24, 2002*

ABSTRACT: An investigation of the structural and dynamic properties of the C-terminal fragment of the human protein VASP (VASP 336−380) has been performed. Full length VASP has been shown to be tetrameric in solution, and the C-terminal 45 residues of the protein have been suggested to be responsible for the oligomerization. We have expressed and purified a C-terminal fragment of the human VASP protein from residue 336−380. It was found to form a stable domain in its own right. The fragment was shown by CD spectroscopy to form a helical structure, stable under a wide range of temperature and pH conditions. A $^{15}$N-HSQC-experiment exhibits only one set of peaks, suggesting a high degree of symmetry for a putative oligomer. Measurements of the rotational correlation time $\tau_C$ of the molecule and analytical ultracentrifugation data show VASP (336−380) to be entirely tetrameric in solution. The secondary structure was confirmed from a $^{15}$N-NOESY-HSQC experiment and is completely α-helical. We conclude that VASP (336−380) forms a tetramer in solution via a coiled coil arrangement and is solely responsible for tetramerization of full-length VASP.

The Ena/VASP[1] family of molecular adaptor proteins are vital components of signal transduction pathways. They are involved in the re-organization of the cytoskeleton and have been identified in recent years as key players in actin filament assembly and cell−cell adhesion processes. These include thrombocyte activation, migration of neuronal growth cones or fibroblasts, motility of intracellular pathogens, and T-cell activation during interaction with accessory cells or formation of epithelial sheets. Ena/VASP proteins support the localized assembly of large multicomponent protein signaling complexes and control effector proteins in an appropriate molarity required for vectorial actin polymerization (for a recent review, see ref *1*). These complexes are regulated largely by predefined protein−protein interactions mediated by networks of protein domains that are present in adaptor and scaffolding proteins.

Ena/VASP proteins share a tripartite domain organization comprising highly conserved EVH1 and EVH2 domains located at the protein N- and C-termini, respectively, separated by a central, low-complexity region which includes a proline-rich segment of 60−90 amino acids in length. The N-terminal EVH1 domains function as localization modules by binding to cognate interaction partners via their exposed, proline-rich, core recognition motifs, with the concensus sequence FPxΦP (where x is any residue and Φ is a hydrophobic residue). The notably low binding affinities (400−500 μM) of EVH1 domains to isolated FPxΦP motifs are increased by interactions with epitopes flanking the ligand core motif (*2*). The proline-rich regions of the Ena/VASP proteins contain GPPPPP motifs in different copy numbers and bind to various effector proteins, including profilin (*3*), which is involved in actin polymerization, and the SH3 and WW domains of a number of other signal transduction proteins (see ref *1* and references cited therein). The C-terminal EVH2 domain has been shown to interact directly with intact F-actin (*4*). The 45 C-terminal residues (VASP 336−380) are highly conserved (Figure 1) and have been implicated in the tetramerization of the Ena/VASP proteins (*4*).

Secondary structure prediction using a hierarchical neural network algorithm (*5*) shows a high probability that the VASP(336−380) monomer possesses a completely α-helical conformation (data not shown). This is in agreement with previous proposals that oligomeric EVH2 may form a coiled coil structure at its C-terminus (*4*). Sequence comparisons with other known coiled coil proteins further support this idea. For example, residues 351−361 of VASP are almost identical in sequence to a sub-sequence of the yeast *retro*-GCN4 leucine zipper (in which the native GCN4 sequence was reversed from C- to N-terminus), which forms a parallel tetrameric coiled coil (*6*). The natural GCN4 leucine zipper, in contrast, forms a dimer (*7*). The sequence homology

† L.J.B. and T.J. are grateful to EMBO and the DFG (Grant Number SFB 355 TP C3) for financial support.

* Corresponding authors. Tel.: ++49 (0) 30-94793 232. Fax: ++49 (0) 30-94793 169. E-mail: L.J.B., ball@fmp-berlin.de; J.Z., zimmermann@fmp-berlin.de.

‡ Forschungsinstitut für Molekulare Pharmakologie.

§ Universität Würzburg.

[1] Abbreviations: CD, circular dichroism; EVH1, Ena/VASP homology 1 domain; EVH2, Ena/VASP homology 2 domain; GST, glutathione S-transferase; IPTG, isopropyl β-D-thiogalactopyranoside; MALDI-TOF MS, matrix assisted laser desorption ionization time-of-flight mass spectrometry; MW, molecular weight; NMR, nuclear magnetic resonance; PRM, proline rich motif; SE, sedimentation equilibrium; SV, sedimentation velocity; UC, ultracentrifugation; VASP, vasodilator stimulated phosphoprotein.

10.1021/bi020379x CCC: $22.00 
Published on Web 08/21/2002

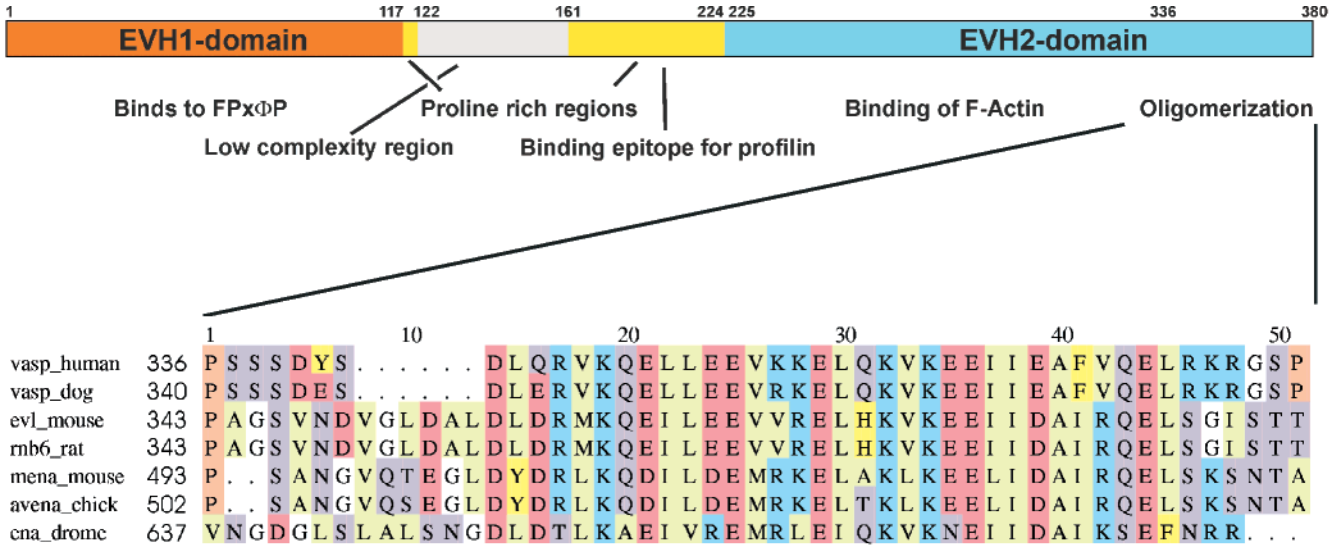


FIGURE 1: Domain organization of VASP and multiple sequence alignment of the C-terminal region of EVH2 domains from different organisms. Swissprot and Trembl database accession codes are p50552 (VASP, *Homo sapiens*), p50551 (VASP, *Canis familiaris*), p70430 (EVL, *Mus musculus*), o08719 (RNB6, *Rattus norvegicus*), p70433 (Mena, *Mus musculus*), o93263 (Avena, *Gallus gallus*), and q24035 (Ena, *Drosophila melanogaster*). The alignment was performed using the Wisconsin package (version 10.0, Genetics Computer Group Inc., Madison, WI). Amino acids are colored as follows: red, acidic; blue, basic; purple, polar; green, hydrophobic; yellow, aromatic; brown, Proline.

between the C-terminal 45 amino acids of EVH2 and other tetrameric coiled coil proteins for which high-resolution structures have now been solved is, however, rather low. Examples are the Mnt repressor from the *Salmonella* phage P22 (*8*), which forms a dimer of two right-handed coiled coil dimers; the NSP4 receptor protein from rotavirus (*9*), which forms a parallel tetrameric coiled coil; and a fragment of the surface layer protein tetrabrachion from the hyperthermophilic archaeon *Staphylothermus marinus* (*10*), which also forms a parallel tetrameric coiled coil.

A potential role of EVH2 mediated oligomerization would be in targeting bundled EVH1 domains to several FPxΦP motifs in target proteins. The binding partners of Ena/VASP proteins containing the EVH1 interaction motif, FPxΦP, are diverse and dependent on the cellular context (*1*, *11*, *12*). The copy number of EVH1-binding motifs in individual proteins varies between 1 and 4 per polypeptide chain. The mammalian zyxin and *Listeria* ActA proteins contain FPxΦP motifs in 4-fold tandem repeat (*13*, *14*), whereas the cytoskeletal EVH1-binding protein vinculin contains only a single copy of the FPxΦP motif (*15*, *16*). The axon guidance receptors Robo and Semaphorin 6A-1 and the adaptor protein Fyb/SLAP, which is involved in T-cell receptor signaling, also each harbor a single functional copy of the EVH1-binding FPxΦP motif (*17*−*19*). This suggests that the overall stoichiometry and composition of complexes varies. EVH1-binding proteins with a single FPxΦP motif could either exist as oligomers (as has been shown for vinculin) or may be oligomerized upon binding to Ena/VASP proteins. Binding of tetradentate Ena/VASP proteins to EVH1-binding proteins with 4-fold repeated FPxΦP motifs, such as zyxin or ActA proteins, could be realized by the formation of 4:1 complexes, where each of the four EVH1 domains from a tetrameric Ena/VASP protein binds to one of the four tandem FPxΦP motifs in a single molecule of the respective zyxin or ActA interaction partner. Alternatively, at the other extreme, each of the four FPxΦP motifs could engage a complete Ena/VASP tetramer, resulting in four VASP tetramers (i.e., 16 VASP monomers) being recruited to each molecule of the interaction partner. Such 16:1 complex formation would allow for the further binding, and thus cross-linking, of different EVH1-binding proteins in oligo-molecular signaling complexes.

We have expressed, isolated, and characterized biophysically a fragment containing the C-terminal 45 residues of the human VASP protein, VASP(336−380). This comprises an independently folded structural element within the extended EVH2 domain. On the basis of detailed deletion analyses on the VASP EVH2 domain, it was suggested that this region is important for tetramerization of full-length VASP (*4*).

## MATERIALS AND METHODS

*Expression and purification of recombinant VASP(336−380) and $^{15}N$ labeling.* The DNA sequence encoding human VASP 336−380 (accession no. Z46389) was cloned into the BamHI and EcoRI site of the pGEX-4T-1 vector (Pharmacia, accession no. U13853), which also codes for ampicillin resistance. *E. coli* BL21 (DE3) cells (Invitrogen) were transformed with this vector and cells were grown at 37 °C on M9 minimal medium containing 100 mg/L ampicillin. The medium was substituted with 0.5 g/L $^{15}NH_4Cl$ without or with 2 g/L uniformly $^{13}C$-labeled glucose for uniformly $^{15}N$- or $^{15}N/^{13}C$-double-labeled samples, respectively. Protein expression was induced by addition of isopropyl-$\beta$-D-thiogalactopyranoside (IPTG) at $OD_{600} = 0.6-0.8$ to a final concentration of 1 mM, and cell growth was continued at 25 °C overnight before harvesting. Cells were lysed by French Press (Amico), and the desired protein was purified on a Glutathione-Sepharose 4B column (Pharmacia) (buffer: NaCl 140 mM, KCl 2.7 mM, $Na_2HPO_4$ 10 mM, $KH_2PO_4$ 1.8 mM, pH 7.3; elution buffer: Tris 50 mM, pH 8.0, glutathione (red.) 3 g/L). The eluted GST-fusion protein was concentrated to 0.2 mM and the GST moiety cleaved by thrombin at RT for 20 h, using 2.5 U thrombin/mg of

fusion protein. The cleaved protein was purified to homogeneity using a Glutathione-Sepharose 4B column, followed by final purification on a Superdex 75 gel filtration column (Pharmacia) (buffer: Tris 50 mM, NaCl 150 mM, pH 8.0). Desired fractions, monitored by UV absorption at 280 nm, were concentrated using a Biomax 3K concentration filter (Millipore) to 500 $\mu$L in NMR buffer (20 mM $KP_i$, 50 mM NaCl, pH 6.0, 0.02 mM $NaN_3$). The cleaved protein contains two additional residues (GS) at the N-terminus, arising from the thrombin cleavage site. The homogeneity and molecular mass of the protein were confirmed by SDS-PAGE and MALDI-TOF MS.

*Circular Dichroism Spectroscopy.* Circular dichroism (CD) spectroscopy was performed on a J-720 spectropolarimeter (Jasco, Tokyo, Japan), using a quartz cuvette with 0.1 cm path length and a protein concentration of 0.025 mg/mL (1.2 $\mu$M) in NMR buffer. Measurements from 200 to 260 nm were performed in the pH range from 1 to 10. A temperature scan from +4° to +80 °C was also performed at 209 nm (the strongest minimum in the protein's CD spectrum). Spectra were analyzed using the program Origin (Microcal, version 5.0).

*NMR spectroscopy and $^{15}N$ relaxation experiments.* A 4.5 mM $^{15}N$-labeled sample of VASP(336−380) was prepared for NMR experiments, containing 10% $D_2O$ for the $^2H$ lock. All NMR spectra were recorded at 300 K, using either Bruker DRX 600 or DMX 750 spectrometers in standard configuration, with triple-resonance probes equipped with triple-axis self-shielded gradient coils. Multidimensional NMR spectra, including 3D $^{15}N$-separated TOCSY (*20*), HNHA, HNHB, and NOESY (*21*) spectra (mixing time 60 ms), were recorded as described in the original references. A 3D $^{15}N$/$^{15}N$-HMQC-NOESY-HSQC spectrum (*22*) was recorded with $^{15}N$ evolution in both indirect dimensions to assist with the assignment of short to medium range $d_{NN}$ NOEs. A ∼4 mM uniformly $^{15}N$/$^{13}C$-labeled sample was used to acquire 3D CBCANNH (*23*), CBCA(CO)NNH (*24*), and HNCO spectra for unambiguous backbone assignment. Due to the low level of dispersion in the $^{15}N$ dimension, digitization in this dimension was optimized using a reduced $^{15}N$ spectral width of 1282.1 Hz (at 600 MHz).

Relaxation properties of backbone amide $H_N$ nuclei were determined by recording series of $^{15}N$ $T_1$ and $T_2$ relaxation experiments (*25*), with randomly ordered relaxation delays to avoid the accumulation of systematic errors. In each case, cross-peak intensities were fitted to a single-exponential decay using the program Sparky (version 3.1, T. D. Goddard and D. G. Kneller, SPARKY 3, University of California, San Francisco). The mean value of the $^{15}N$ $T_1$ and $T_2$ over residues 10−44 was then used for calculation of the correlation time $\tau_C$, using eq 1 (*26*):

$$\tau_C = \frac{\left\{[6(T_1/T_2) - 7]\frac{1}{4}\right\}^{1/2}}{\Omega_N \cdot 2\pi} \quad (1)$$

where $T_1$ and $T_2$ are the mean trimmed $^{15}N$ relaxation times (*26*) and $\Omega_N$ is the Larmor frequency of $^{15}N$ at the field strength used (60.827 865 MHz in the present study).

All NMR data were processed using the XWIN-NMR program (version 2.6) of Bruker Analytik GmbH (Rheinstetten, Germany) and the AZARA (version 2.1) program of W. Boucher (unpublished). Assignment was carried out using the user-interactive program ANSIG 3.3 (*27*, *28*) on a Silicon Graphics O2 workstation. AZARA and ANSIG are both available by anonymous ftp from http://ftp.bio.cam.ac.uk in the directory ftp/pub.

*Analytical ultracentrifugation.* Both sedimentation velocity (SV) and sedimentation equilibrium (SE) experiments were performed with a Beckman Xl-I analytical ultracentrifuge using a 4 hole An-60 Ti rotor of radius 6.5 cm (i.e., from rotor center to cell center). Cells were equipped with 12 mm double-sector, aluminum-filled Epon centerpieces and quartz windows. The absorption optics of the instrument was used at suitable wavelengths for detection of the gradient. A stock solution of VASP(336−380) was concentrated using an Centricon concentrator (Millipore) with a MW cutoff of 3000 Da. Solutions with concentrations of 0.25, 0.125, and 0.0625 mM (i.e., 5.3, 2.6, and 1.3 mg/mL) were prepared using the flow-through as diluent. The partial specific volume ($\bar{v}$) of the protein was calculated from the sequence to be 0.7384 $cm^3/g$, using the consensus partial volumes of amino acids as given in the literature (*29*). The extinction coefficient at 280 nm was calculated to be 1280 A $mol^{-1}$ $cm^{-1}$ from the sequence (*30*) and the values for the other wavelengths calculated relative to that value from a wavelength spectrum. (Values for the density and viscosity of the buffer were calculated using the options provided in the Software package UltraScan 5.0 by B. Demeler, PhD UTHSCSA, USA. Viscosity was 1.0169 cp at 20 °C, and density was 1.0098 g/mL.)

SV experiments were performed at 20 °C and 45 000 rpm with 300 $\mu$L of protein solution in each of three cells. Sedimentation scans were acquired every 180 s at 238 nm. Sedimentation and diffusion coefficients were computed using the program LAMM (*31*), which uses direct fitting of the distribution curves according to the Lamm equation (*32*).

SE experiments were performed with 100 $\mu$L of protein solution. After 2 h 30 min of overspeeding at 40 000 rpm, the sample was then spun at 28 000 rpm for 36 h before acquiring the equilibrium gradients at 260 nm, respectively. SE data were analyzed using the program POLYMOLE (*33*).

## RESULTS

To investigate the oligomeric nature of the VASP (336−380) EVH2 domain, we derived its secondary structure by CD and NMR and determined the aggregate size by analytical ultracentrifugation experiments and NMR $^{15}N$ relaxation experiments.

*pH and temperature dependence of the VASP(336−380) secondary structure investigated by CD.* CD spectroscopy of VASP(336−380) was performed at different pH values and temperatures to investigate the stability and secondary structure of the construct. The CD spectra showed all characteristics of a helical conformation with minima at 209 and 222 nm (data not shown). The protein was highly stable, remaining fully folded from pH 1 to 10 (at 24 °C), and within a temperature range of 4−80 °C (at pH 6.0), thus allowing a wide range of stable conditions under which further investigations could be carried out.

*Resonance assignment, secondary structure, and molecular symmetry of VASP(336−380).* The 600 MHz $^{15}N$−HSQC spectrum of VASP(336−380) at pH 6.0 and 300 K is shown

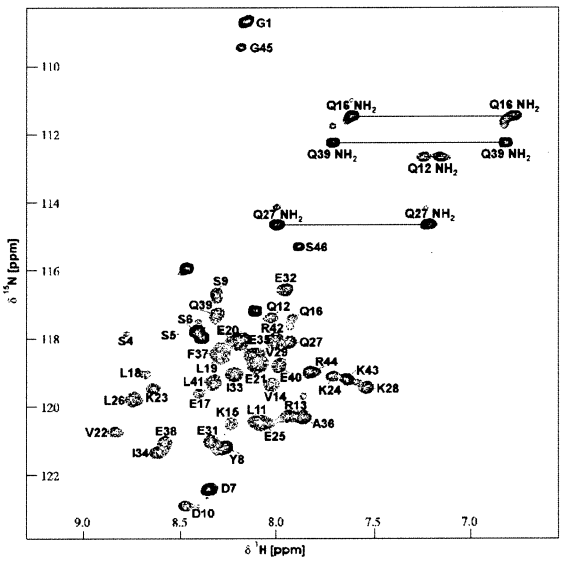


FIGURE 2: $^{15}$N−HSQC spectrum of a 5 mM uniformly $^{15}$N-labeled sample of VASP(336−380) at 300 K (the construct contains additional GS residues at the N-terminus from the thrombin cleavage site). Backbone amides for 43 out of 45 nonproline residues were assigned unambiguously. Peaks connected by a line indicate Gln side chain $NH_2$ group resonances. A single set of peaks shows that the molecule must possess either one 4-fold ($C_4$) or two 2-fold axes of symmetry ($C_{22}$).

in Figure 2. It was possible to assign 43 out of the 47 residues (two of which were prolines). To resolve the spectral overlap, a 3D-NOESY-HSQC spectrum was recorded. Together with use of the 3D CBCA(CO)NNH and CBCANNH spectra, this allowed an almost complete set of $^{15}$N, $^{1}$HN, $^{13}$C$\alpha$, and $^{13}$C$\beta$ assignments to be obtained.

The presence of a single set of peaks in the HSQC spectrum (Figure 2) indicates the magnetic equivalence of the monomeric units of any oligomers present. For a tetramer, this limits the possible symmetry arrangements to either $C_4$ or $C_{22}$ symmetry groups. In all other arrangements, monomers in different environments would experience distinct chemical shifts, resulting in multiple sets of $^{1}$H-$^{15}$N peaks. For example, the $C_2$ symmetry of the tetrameric Mnt repressor results in two sets of $^{1}$H-$^{15}$N peaks in the spectra (*8*). In such cases, nuclei in different monomers experience different chemical environments, and their signals may differ in frequency by up to several ppm. Our spectra show clearly the VASP(336−380) tetramer to possess either $C_4$ symmetry (a parallel four-helix, coiled coil arrangement) or $C_{22}$ symmetry (a symmetrical dimer of symmetrical dimers, *34*).

The NOE connectivity pattern shown in Figure 3, obtained from the 3D-NOESY-HSQC spectrum, clearly indicates an α-helical structure for VASP(336−380), in agreement with our CD data. This is further corroborated by deuterium exchange experiments, which yield a series of slowly exchanging amide hydrogens, also marked on the Figure.

*$^{15}$N relaxation behavior and molecular correlation time ($\tau_C$) of VASP(336−380).* To investigate the self-association behavior of VASP(336−380) and to study the dependence of oligomerization on the protein concentration, we used a series of $^{15}$N $T_1$ and $T_2$ relaxation experiments to determine the average correlation time of the fragment at different protein concentrations. The concentrations studied ranged between 0.25 and 5.0 mM. The relaxation properties shown in Figure 4a demonstrate clearly that VASP(336−380) is highly structured in the range 346−377 with little internal mobility, except at the extreme N- and C-termini of the construct. This is in agreement with heteronuclear $^{15}$N-$^{1}$H NOE experiments, carried out at the same concentrations (data not shown). The average $^{15}$N $T_1$, $T_2$, and calculated molecular correlation times, $\tau_C$, at total protein concentrations 0.25, 0.625, 1.25, 2.5, and 5.0 mM are shown in Table 1. The average $\tau_C$ of 18.9 ns over the five concentrations measured by NMR can be attributed to a molecular mass of ∼20−22 kDa within the limits of experimental error (see Figure 4b). As there is no precise simple relationship between correlation time and molecular mass of a protein, this plot yields only a rough estimate of the mass. The correlation time is also related to overall molecular shape. For an elongated molecule, we would expect a larger $\tau_C$ than for a globular molecule of the same molecular mass. The calculated $\tau_C$ is in reasonable agreement with the theoretical molecular weight of 21.5 kDa for tetrameric VASP(336−380). Furthermore, despite a 20-fold difference between the maximum and minimum protein concentrations measured, the overall $\tau_C$ remained constant within the limits of experimental error (Figure 4c). We therefore conclude from these data, that VASP(336−380) is fully tetrameric in solution and that this state is independent of the protein concentration in the range 0.25−5.0 mM. This agrees well with our previous studies using 1,1-ECHO experiments (*35*), which yielded an approximate correlation time of 14 ns for the molecule (data not shown).

*Molecular mass determination and analysis of equilibrium oligomer populations by analytical ultracentrifugation.* The relative equilibrium populations of VASP(336−380) oligomers at a series of different protein concentrations and temperatures were investigated by analytical ultracentrifugation. Concentrations studied were 0.0625, 0.125, and 0.25 mM, each at 10, 20, and 27 °C. From sedimentation velocity (SV) experiments (see Figure 5), the sedimentation co-

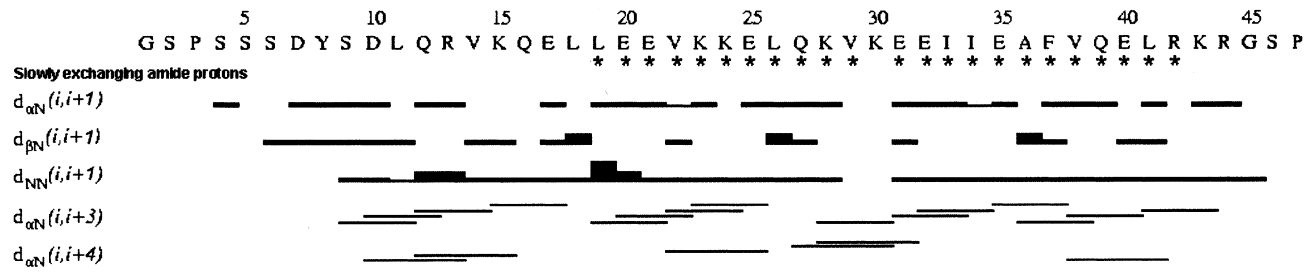


FIGURE 3: NOE connectivity pattern of VASP (336−380) from the 3D $^{15}$N-NOESY spectrum (as obtained from ANSIG). The backbone HN−HN and HN−C$\alpha$ connectivities are characteristic of α-helical structure. Some expected connections are missing due to resonance overlap. Slowly exchanging amide protons are marked with an asterisk.

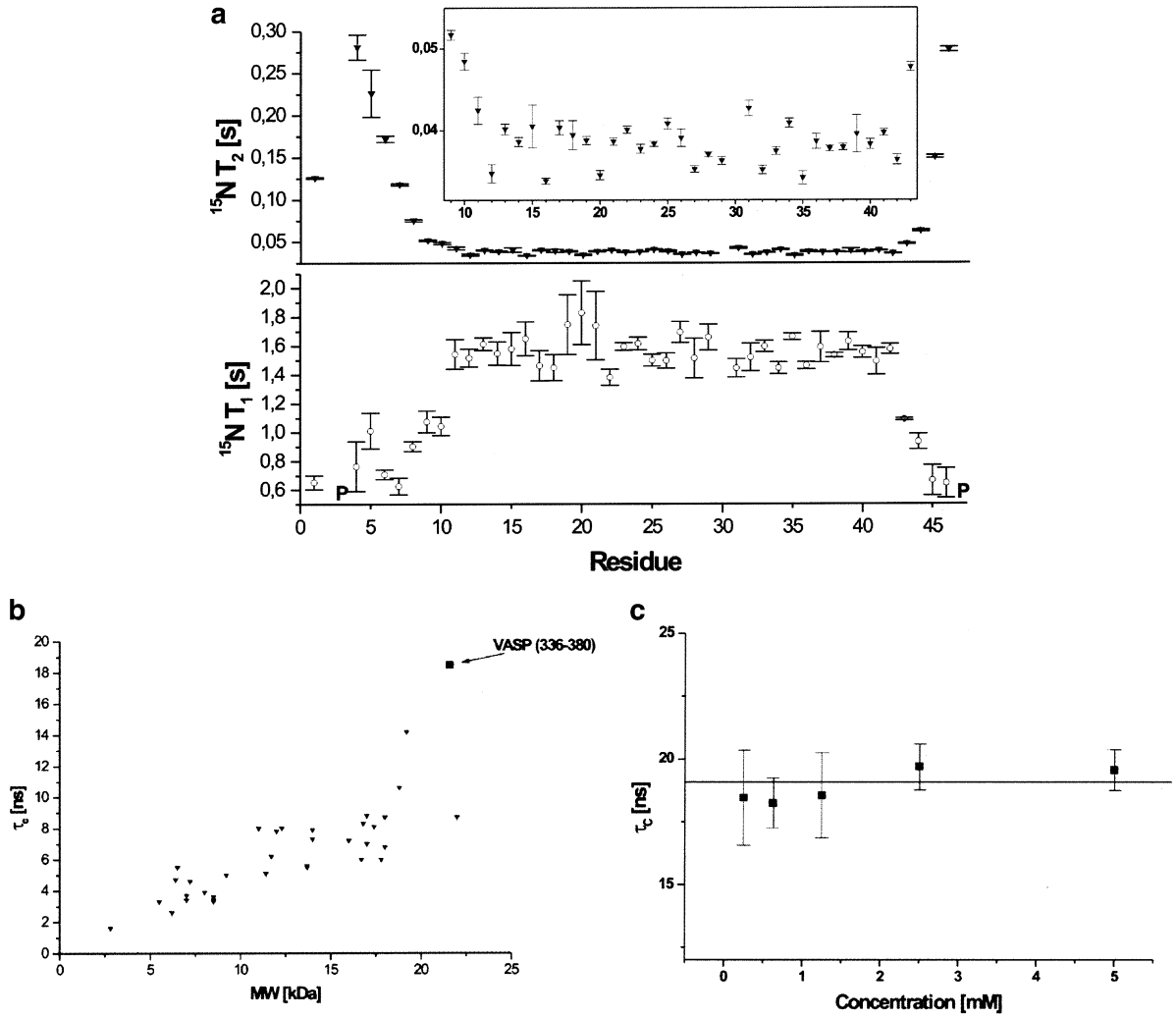


FIGURE 4: (a) Plot of $^{15}$N relaxation time constants, $T_1$ and $T_2$, for each residue of VASP(336−380), shown for a protein concentration of 5 mM (inset: extension of $T_2$ for residues 9−43). The protein is motionally restricted in the core region (residues 10−44, corresponding to aa 346−377 of VASP numbering) with some flexibility observed at the N- and C-termini. (b) Plot of the correlation time $\tau_C$ for different proteins versus molecular weight. Values for the reference proteins were taken from the literature (*45*). Variations from linearity show that not only MW but also molecular shape affects the overall correlation time in solution. The correlation time for VASP(336−380) is marked on the plot (square box) and is in good agreement with an expected MW of ~22 kDa, corresponding to a tetramer. (c) Dependence of the molecular correlation time of VASP(336−380) on concentration. The mean value of $\tau_C$ from the five concentrations measured (see Table 1) was 18.9 ns. The $\tau_C$ was calculated for the motionally restricted residues 10−44 (VASP(346−377)). Residues with a $T_1$ or $T_2$ deviating by more than one standard deviation from the mean were not considered in this calculation (*26*). $\tau_C$ is practically constant over the concentration range under investigation, indicating that the oligomerization state is unchanged and predominantly tetrameric between 0.25 and 5 mM (P = Proline).

Table 1: Summary of $T_c$ Determination and MW Prediction from $\tau_C$ by UC Measurements (SD Given in Parentheses)[a]

| concentration (mM) | $T_1$ (ms) | $T_2$ (ms) | $\tau_C$ (ns) | MW (Da) |
|---|---|---|---|---|
| 5.0 | 1521.2 (78.4) | 39.6 (0.8) | 19.6 (0.8) | – |
| 2.5 | 1513.7 (71.1) | 38.8 (0.7) | 19.7 (0.8) | – |
| 1.25 | 1481.3 (184.6) | 42.7 (3.2) | 18.6 (1.7) | – |
| 0.625 | 1433.2 (255.6) | 42.7 (3.2) | 18.3 (1.0) | – |
| 0.25 | 1083.9 (606.7) | 31.6 (11.3) | 18.5 (1.9) | 20 290 (243) |
| 0.125 | – | – | – | 20 600 (421) |
| 0.0625 | – | – | – | 21 250 (795) |

[a] The oligomerization state of VASP(336−380) was determined over a broad concentration range, from 0.0625 to 5mM, using both NMR measurements of the correlation time $\tau_C$ and analytical ultracentrifugation. Both methods yield results in close agreement for all concentrations investigated.

efficient, *s*, was found to be 1.98 S (1 S = $10^{-13}$ s), and from sedimentation equilibrium (SE) experiments (Figure 6), a molecular mass (averaged over all concentrations and temperatures studied) of 21.9 Da was calculated for the detected species. This is in excellent agreement with a predicted molecular weight of 21 988 Da for a $^{15}$N-labeled VASP(336−380) tetramer.

Additionally, these parameters allowed us to calculate the diffusion coefficient (*D*) using the Svedberg equation

$$M = \frac{sRT}{D(1 - \rho\bar{v})} \quad (1)$$

where *s* is the sedimentation coefficient, *M* the molecular mass, $\bar{v}$ the partial specific volume of the solute, $\rho$ the density of the solvent, *R* the ideal gas constant, and *T* the temperature. The diffusion coefficient (*D*) was calculated to be $8.703 \times 10^{-7}$ (cm$^2$/s). On the basis of eq 2, it was then possible to specify the frictional ratio, $f/f_0$, for the unhydrated protein:

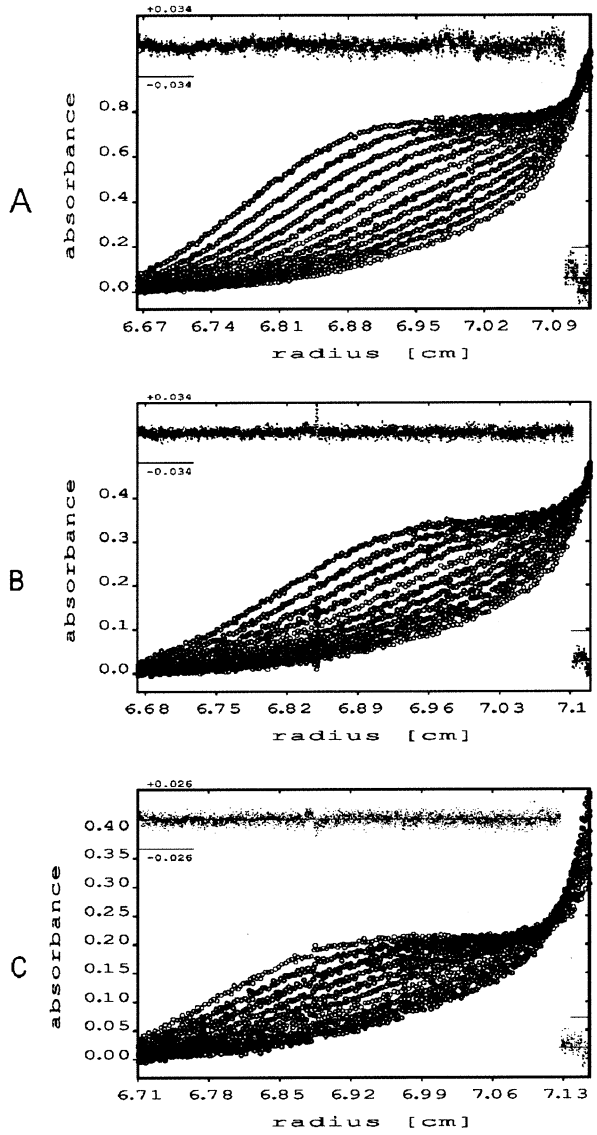


FIGURE 5: Radial absorbance distributions of sedimentation velocity experiments and fitted data of 0.25 (a), 0.125 (b), and 0.0625 mM (c) VASP(336−380) in NMR buffer (see methods). The profiles were recorded at 286 nm with time differences of 180 s. The temperature was 20 °C and the speed 45 000 rpm. Residuals (indicating the rmsd of the data to the fit) as shown along the top of each plot are of all datasets and given in 2-fold amplification and scaled according to the axis marked on the plots. Calculated sedimentation coefficient (*s*), for each concentration were (a) 2.01, (b) 1.96, and (c) 1.97 S, with an average of 1.98 S (S $=10^{-13}$ s).

$$f/f_0 = 10^{-8}\left[\frac{1-\rho\bar{v}}{sD^2\bar{v}}\right]^{1/3} \quad (2)$$

where $f$ is the frictional coefficient of the protein and $f_0$ is the ideal frictional coefficient for a perfectly spherical molecule (defined as 1.0). From this we obtained a value of 1.32 for the frictional ratio $f/f_0$ of the protein, implying that its overall conformation deviates significantly from spherical. Prediction of the molecular dimensions from the molecular mass and *s* value yielded possible axis ratios (longest axis/shortest axis) of 6.00, 6.09, and 6.87, for long-rod, prolate, and oblate models, respectively. These values are highly dependent on the accuracy of *D* and therefore give only an estimate of the molecular shape. Although it is not possible to distinguish which of these three different models corresponds to the VASP(336−380) EVH2 tetramer arrangement on the basis of these data alone, it is clear that the molecule possesses a considerably elongated overall structure.

In the SE experiments, the concentration gradients yielded a MW of 21.9 kDa irrespective of protein concentration and temperature (Figure 7), indicating that a single oligomer species is present as opposed to an equilibrium mixture of different oligomers. The average value obtained for the MW corresponds closely to a tetramer of VASP(336−380), is in excellent agreement with the result obtained from the SV experiments, and agrees well with the results of our $^{15}$N relaxation experiments. A number of different models were tested in order to determine the nature of the oligomerization equilibrium. Within the concentration range used, no other component than the tetramer could be detected in the SE gradients. We therefore conclude that VASP(336−380) behaves as a single, ideal, tetrameric entity under the range of conditions examined, suggesting a very low dissociation constant of the oligomer.

## DISCUSSION

Protein−protein interactions in signal transduction complexes must be tightly regulated. This can be achieved in a number of independent, but complementary ways. Interactions of the EVH1 domains with their target proline rich peptides are generally of very low affinity. Stoichiometry and entropic influences can also act as regulatory factors enhancing interaction affinities. The EVH2 domain of the Ena/VASP proteins may thus be important for strengthening these interactions via oligomer formation.

The frequency and distribution of PRM's in the primary sequences of their host proteins and the oligomerization states of both interaction partners thus provide clues about the possible stoichiometry of the complexes formed. For example, the four EVH1-binding FPxΦP repeats in zyxin and ActA contrast with the single FPxΦP copy in vinculin and other EVH1-binding proteins. The oligomerization state of zyxin is monomeric (*36*). This is in contrast to vinculin, which is known to multimerize (*16*, *37*). The ActA protein has been shown to exist in either monomeric (*38*) or dimeric states (*39*). We have shown here that an isolated, highly conserved structural element comprising VASP(336−380) forms a tetramer in solution. We conclude that this element is responsible for tetramerization of the full length VASP molecule which has previously been shown to form a tetramer (*40*). In light of the available data, different stoichiometries and composition of complexes between tetrameric VASP (and, by inference, of Ena/VASP proteins) and its FPxΦP-containing binding partners may be envisaged. Binding of tetradentate VASP to EVH1-binding proteins with 4-fold repeats of the FPxΦP motif could result in either the formation of a 4:1 complex or a 16:1 complex, depending on the mode of binding.

EVH1-binding proteins with single copy FPxΦP motifs may either exist as oligomers in their own right (as has been observed for vinculin) or may become oligomerized upon binding. Tetramerization thus renders VASP a potential tetradentate ligand for its different binding partners and this could provide an independent mechanism for increasing not only the binding affinity of the otherwise low-affinity

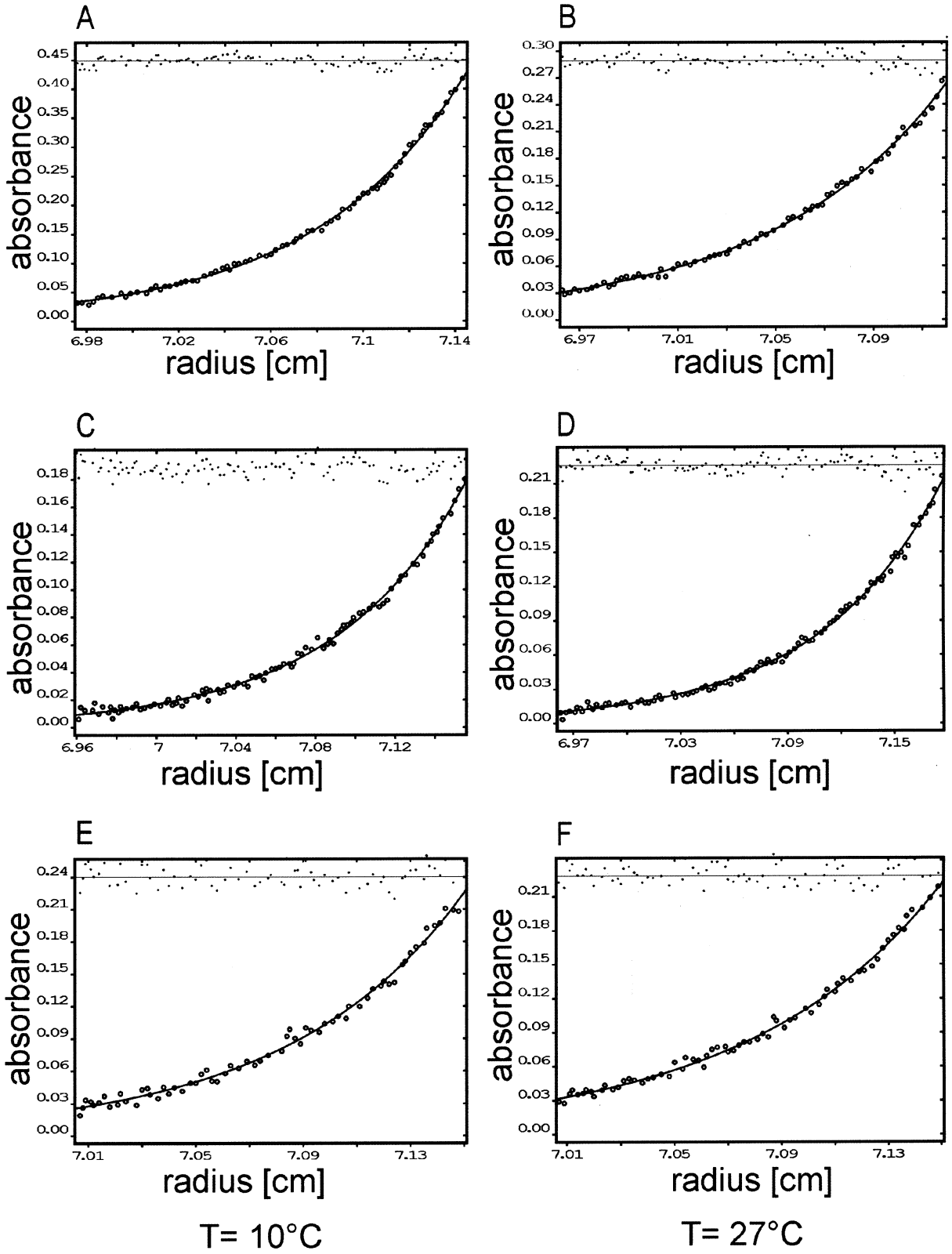


FIGURE 6: Radial concentration distribution curves from sedimentation equilibrium experiments of VASP(336−380) in NMR buffer (see methods). The profiles were recorded at 260 nm after 36 h equilibration at a speed of 28 000 rpm. The curves were fitted using the program POLYMOLE (*33*). The two vertical panels show data for temperatures 10 °C (A, C, E) and 27 °C (B, D, F), respectively. Data acquired at 20 °C are not shown. The concentrations are as follows: 0.25 mM (plots A and B), 0.125 mM (plots C and D) and 0.0625 mM (plots E and F). Residuals calculated from all datasets are shown above each plot, in 2-fold amplification and scaled separately according to the axis marked on the plots.

interaction with PRM-containing proteins but also facilitate the local concentration of effector proteins such as profilin or F-actin during targeted microfilament re-organization. Evidence in favor of such affinity-modulating effects has been described with an *ena* allele encoding a mutant protein that lacks the C-terminal 49 amino acids. This oligomeriza-

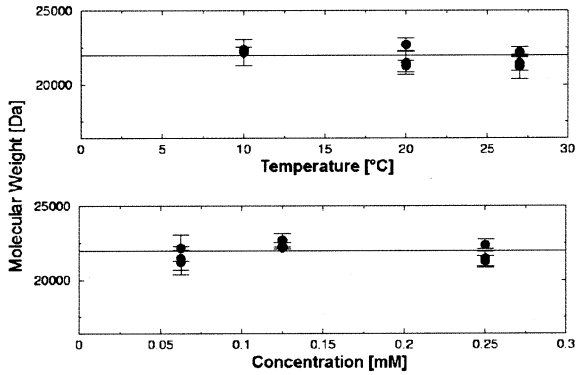


FIGURE 7: Consistency of calculated MW from sedimentation equilibrium of VASP(336−380) with temperature and protein concentration. Within the limits of error, no notable variations in average MW were observed.

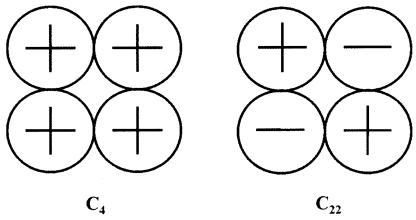


FIGURE 8: Possible symmetry arrangements for the tetramer. The four monomers may be arranged either all parallel ($C_4$) or in a head-to-tail arrangement ($C_{22}$).

tion-deficient mutant is impaired in its interaction with zyxin and an Abl-SH3 domain despite the presence of the corresponding binding regions in its amino acid sequence (*41*). VASP constructs with the proposed F-actin binding site but lacking the C-terminal 40 amino acids displayed considerably reduced F-actin binding affinity *in vitro* and *in vivo* (*4*). Similarly, deletion of residues 285−380 of VASP affects EVH1 domain mediated interactions by impairing its subcellular localization to focal adhesions (*40*).

The symmetry of the tetrameric VASP may play an important role in complex formation with different interaction partners by imposing proximity and directional constraints on the architecture of the signaling complexes formed. Our NMR data revealed a high degree of symmetry in the tetramerization domain of VASP, which could be interpreted in two ways. The two possible types of symmetry are depicted in Figure 8. The first is a $C_4$ symmetric arrangement with all four strands parallel to each other. The second is a $C_{22}$ symmetric arrangement, with alternating head-to-tail contacts. A parallel, coiled-coil arrangement of monomers with a $C_4$ rotational axis would align the four VASP molecules so that their EVH1 domains were oriented in the same direction. However, if the C-termini arranged themselves into an antiparallel tetramer, with $C_{22}$ symmetry, this spatial arrangement would favour separation of intra-tetramer EVH1 domains and facilitate the formation of cross-links between EVH1-binding proteins of the same or of different type. The frictional ratio of 1.32 obtained from our studies indicates that the overall arrangement of the VASP(336−380) tetramer is rather elongated. This would be in agreement with a structure of the type observed for other tetrameric coiled coils. (For a recent review on coiled coil motifs, see ref *42*.) The detailed analysis of NOE data does not show obvious head-to-tail connections, which hints at a $C_4$ arrangement. This question will only be settled when the three-dimensional tetramer structure has been determined. Work to this end is currently in progress.

The methods used in this work to study VASP oligomerization provided highly complementary information on the thermodynamic stability of VASP(336−380). The $^{15}N$ relaxation experiments were valuable for studying the oligomerization behavior of VASP(336−380) at higher protein concentrations (up to 5 mM), whereas analytical ultracentrifugation provided data at lower concentrations (down to 0.0625 mM). Independent use of these techniques showed clearly that VASP(336−380) exists exclusively as a tetrameric species under all conditions of temperature and protein concentration studied, with no detectable presence of any other oligomeric species at equilibrium. This observation may be of direct importance for understanding the molecular basis of the pronounced dominant negative effects of VASP EVH2 fragments harboring amino acids 336−380 on VASP-mediated cellular processes such as epithelial or endothelial barrier formation (*43*, *44*). These dominant negative effects have been attributed to mixed tetramer formation of the N-terminal truncated VASP fragment with wild-type protein thereby perturbing its function. However, formation of mixed tetramers seems to be highly unlikely in light of the thermodynamic stability of tetrameric VASP(336−380) described here. Thus, instead of formation of mixed tetramers, competitive sequestration of binding partners by tetrameric EVH2 fragments might be a molecular basis of the dominant-negative effects observed in cell culture and in transgenic animals.

We conclude that the VASP tetramerization domain is a highly conserved structural scaffolding element in its own right, capable of forming highly stable and symmetric tetramers with the function of promoting tetramerization of the intact VASP protein. This in turn suggests important regulatory implications for the function and interactions of this family of proteins in their different multicomponent signaling complexes by increasing the affinity and avidity of the underlying protein−protein interactions.

## ACKNOWLEDGMENT

We thank Martina Leidert and Anne Diehl for their valuable assistance with the preparation of VASP(336-380) protein samples, Peter Schmieder for help with NMR spectra acquisition, Joachim Behlke for his helpful advice regarding interpretation of analytical ultracentrifugation experiments, Eberhard Krause for mass spectrometry, and Mark Kelly for insightful discussions.

## REFERENCES

1. Renfranz, P. J., and Beckerle, M. C. (2002) *Curr. Opin. Cell Biol. 14*, 88−103.
2. Ball, L. J., Kühne, R., Hoffmann, B., Häffner, A., Schmieder, P., Volkmer-Engert, R., Hof, M., Wahl, M., Schneider-Mergener, J., Walter, U., Oschkinat, H., and Jarchau, T. (2000) *EMBO J. 19*, 4903−4914.
3. Reinhard, M., Giehl, K., Abel, K., Haffner, C., Jarchau, T., Hoppe, V., Jockusch, B. M., and Walter, U. (1995) *EMBO J. 14*, 1583−1589.
4. Bachmann, C., Fischer, L., Walter, U., and Reinhard, M. (1999) *J. Biol. Chem. 274*, 23549−23557.
5. Guermeur, Y. (1997) http://pbil.univ-lyon1.fr/pbil.html.

6. Mitti, P. R. E., Deillon, C., Sargent, D., Liu, N., Klauser, S., Thomas, R. M., Gutte, B., and Grütter, M. G. (2000) *Proc. Natl. Acad. Sci. 97*, 2562−2566.
7. Junius, F. K., O'Donoghue, S. I., Nilges, M., Weiss, A. S., and King, G. F. (1996) *J. Biol. Chem. 271*, 13663−13667.
8. Nooren, N. M. A., Kaptein, R., Sauer, R. T., and Boelens, R. (1999) *Nat. Struct. Biol. 6*, 755−759.
9. Bowman, G. D., Nodelman, I. M., Levy, O., Lin, S. L., Tian, P., Zamb, T. J., Udem, S. A., Venkataraghavan, B., and Schutt, C. E. (2000) *J. Mol. Biol. 304*, 861−871.
10. Stetefeld, J., Jenny, M., Schulthess, T., Langwehr, R., Engel, J., and Kammerer, R. A. (2000) *Nat. Struct. Biol. 7*, 772−776.
11. Ball, L. J., Jarchau, T., Oschkinat, H., and Walter, U. (2002) *FEBS Lett. 513*, 45−52.
12. Reinhard, M., Jarchau, T., and Walter, U. (2001) *Trends Biochem. Sci. 26*, 243−249.
13. Drees, B., Friederich, E., Fradelizi, J., Louvard, D., Beckerle, M. C., and Golsteyn, R. M. (2000) *J. Biol. Chem. 275*, 22503−11.
14. Niebuhr, K., Ebel, F., Frank, R., Reinhard, M., Domann, E., Carl, U. D., Walter, U., Gertler, F. B., Wehland, J., and Chakraborty, T. (1997) *EMBO J. 16*, 5433−5444.
15. Reinhard, M., Rüdiger, M., Jokusch, B. M., and Walter, U. (1996) *FEBS 399*, 103−107.
16. Hüttelmaier, S., Mayboroda, O., Harbeck, B., Jarchau, T., Jockusch, B. M., and Rüdiger, M. (1998) *Curr. Biol. 8*, 479−488.
17. Bashaw, G. J., Kidd, T., Murray, D., Pawson, T., and Goodman, C. S. (2000) *Cell 101*, 703−715.
18. Klostermann, A., Lutz, B., Gertler, F., and Behl, C. (2000) *J. Biol. Chem. 275*, 39647−39653.
19. Krause, M., Sechi, A. S., Konradt, M., Monner, D., Gertler, F. B., and Wehland, J. (2000) *J. Cell Biol. 149*, 181−194.
20. Bax, A., Clore, M., and Gronenborn, A. (1990) *J. Magn. Reson. 88*, 425−431.
21. Clore, M., and Gronenborn, A. (1991) *Prog. NMR Spectrosc. 23*, 43−92.
22. Ikura, M., Bax, A., Clore, M., and Gronenborn, A. (1990) *J. Am. Chem. Soc. 24*, 9020−9022.
23. Grzesiek, S., and Bax, A. (1992) *J. Magn. Reson. 99*, 201−207.
24. Grzesiek, S., and Bax, A. (1992) *J. Am. Chem. Soc. 114*, 6291−6293.
25. Farrow, N. A., Zhang, O., Forman-Kay, J. D., and Kay, L. E. (1997) *Biochemistry 36*, 2390−2402.
26. Gryk, M. R., Abseher, R., Simon, B., Nilges, M., and Oschkinat, H. (1998) *J. Mol. Biol. 280*, 879−896.
27. Kraulis, P. J. (1994) *Biochemistry 33*, 3515−3531.
28. Kraulis, P. J. (1989) *J. Magn. Reson. 24*, 627−633.
29. Behlke, J. (1996) in *Methoden in der Proteinanalytik* (Holtzhauer, M., Ed.) pp 230−275, Springer, Berlin.
30. Gill, S. C., and von Hippel, P. H. (1989) *Anal. Biochem. 182*, 319−326.
31. Behlke, J., and Ristau, O. (1998) *J. Biophys. Chem. 70*, 133−146.
32. Lamm, O. (1929) *Ark. Mater. Astron. Fys. 21B*, 1−4.
33. Behlke, J., and Ristau, O. (1997) *Biochemistry 36*, 5149−5156.
34. Lee, W., Harvey, T. S., Yin, Y., Yau, P., Litchfield, D., and Arrowsmith, C. H. (1994) *Nat. Struct. Biol. 1*, 877−890.
35. Anglister, J., Grzesiek, S., Ren, H., Klee, C. B., and Bax, A. (1993) *J. Biomol. NMR 3*, 121−126.
36. Crawford, A. W., and Beckerle, M. C. (1991) *J. Biol. Chem. 266*, 5847−5853.
37. Molony, L., and Burridge, K. (1985) *J. Cell Biochem. 29*, 31−36.
38. Machner, M. P., Urbanke, C., Barzik, M., Otten, S., Sechi, A. S., Wehland, J., and Heinz, D. W. (2001) *J. Biol. Chem. 276*, 40096−40103.
39. Mourrain, P., Lasa, I., Gautreau, A., Gouin, E., Pugsley, A., and Cossart, P. (1997) *Proc. Natl. Acad. Sci. 94*, 10034−10039.
40. Haffner, C., Jarchau, T., Reinhard, M., Hoppe, J., Lohmann, S. M., and Walter, U. (1995) *EMBO J. 14*, 19−27.
41. Ahern-Djamali, S. M., Comer, A. R., Bachmann, C., Kastenmeier, A. S., Reddy, S. K., Hua, P., Beckerle, M. C., Walter, U., and Hoffmann, F. M. (1998) *Mol. Biol. Cell 9*, 2157−2171.
42. Burkhard, P., Stetefeld, J., and Strelkov, S. V. (2001) *Trends Cell Biol. 11*, 82−88.
43. Vasioukhin, V., Bauer, C., Yin, M., and Fuchs, E. (2000) *Cell 100*, 209−219.
44. Comerford, K. M., Lawrence, D. W., Synnestvedt, K., Levi, B. P., and Colgan, S. P. (2002) *FASEB J.16*, 583−585.
45. Dayie, K. T., Wagner, G., and Lefèvre, J.-F. (1996) *Annu. Rev. Phys. Chem. 47*, 243−282.


BI020379X